Monthly Notices
of the
ROYAL ASTRONOMICAL SOCIETY

MNRAS **454,** 550–559 (2015) doi:10.1093/mnras/stv1938

# The Milky Way system in Λ cold dark matter cosmological simulations

Qi Guo,[1,2]★ Andrew P. Cooper,[2] Carlos Frenk,[2] John Helly[2] and Wojciech A. Hellwing[2,3]

[1]*National Astronomical Observatories, Chinese Academy of Sciences, 20A Datun Road, Chaoyang, Beijing 10012, China*
[2]*Institute for Computational Cosmology, University of Durham, South Road, Durham DH1 3LE, UK*
[3]*Interdisciplinary Centre for Mathematical and Computational Modeling (ICM), University of Warsaw, ul. Pawińskiego 5a, PL-02-106 Warsaw, Poland*

Accepted 2015 August 18. Received 2015 August 18; in original form 2015 March 29

## ABSTRACT

We apply a semi-analytic galaxy formation model to two high-resolution cosmological *N*-body simulations to investigate analogues of the Milky Way system. We select these according to observed properties of the Milky Way rather than by halo mass as in most previous work. For disc-dominated central galaxies with stellar mass (5–7) $\times\ 10^{10}\,\mathrm{M}_{\odot}$, the median host halo mass is $1.4\times10^{12}\,\mathrm{M}_{\odot}$, with 32–68 per cent percentile spread in the range $[0.86, 3.1]\times10^{12}\,\mathrm{M}_{\odot}$, consistent with dynamical measurements of the Milky Way halo mass. For any given halo mass, the probability of hosting a Milky Way system is low, with a maximum of ∼20 per cent in haloes of mass $\sim10^{12}\,\mathrm{M}_{\odot}$. The model reproduces the *V*-band luminosity function and radial profile of the bright ($M_V < -9$) Milky Way satellites ($r < 280$ kpc). Galaxy formation in low-mass haloes is found to be highly stochastic, resulting in an extremely large scatter in the relation between $M_V$ (or stellar mass) for satellites and the depth of the subhalo potential well in which they live, as measured by the maximum of the rotation curve, $V_{\rm max}$. Following Sawala et al., we account for baryonic effects on the growth of dark halo potentials by rescaling $V_{\rm max}$. This adjustment alleviates the 'too big to fail' problem – we find that, in 35 per cent of Milky Way-like systems, three or fewer of the top 12 satellites (in order of $V_{\rm max}$) have $V_{\rm max} > 30\,\mathrm{km\,s^{-1}}$. Our model predicts that around half of the dark matter subhaloes with $V_{\rm max} > 20\,\mathrm{km\,s^{-1}}$ host satellites fainter than $M_V = -9$ and so may be missing from existing surveys.

**Key words:** galaxies: dwarf – galaxies: formation – galaxies: haloes – galaxies: kinematics and dynamics – Local Group – dark matter.

## 1 INTRODUCTION

The cold dark matter (CDM) model has been shown to be consistent with many observations on cosmological scales, but uncertainties remain on small scales where complex baryonic processes are involved. A substantial number of faint satellite galaxies are known in the Milky Way (MW) system. Thanks to their relative proximity, the distribution, chemistry and motions of their individual stars can be measured precisely. This makes the MW satellites an excellent laboratory to test the CDM model and also to investigate the physics of galaxy formation on small scales.

It has been known for some time that the count of substructures in simulated MW-mass dark matter haloes greatly exceeds that of the known luminous MW satellites (e.g. Klypin et al. 1999; Moore et al. 1999). In the context of CDM this is readily explained if the efficiency with which baryons are converted into stars drops quickly at low halo masses. This inefficiency is expected on the basis of the well-understood atomic physics governing radiative cooling, the existence of an ionizing cosmic ultraviolet (UV) background and comparison of the energy released by supernovae (which drive the expulsion of baryons from dark matter haloes) to the depth of halo potential wells (Efstathiou 1992; Kauffmann, White & Guiderdoni 1993; Bullock, Kravtsov & Weinberg 2000; Benson et al. 2002; Somerville 2002). CDM galaxy formation models which incorporate even these most basic astrophysical effects have been able to reproduce not only the abundance but also radial distribution of satellites around the MW (e.g. Li, De Lucia & Helmi 2010; Macciò et al. 2010; Okamoto et al. 2010; Font et al. 2011; Guo et al. 2011; Parry et al. 2012). A host of other effects, such as cosmic ray pressure, may contribute to the regulation of star formation in these most marginal systems (Wadepuhl & Springel 2011).

Dwarf spheroidal galaxies (dSphs) make up most of the MW satellite population. Since they are dark-matter-dominated galaxies,

★ E-mail: guoqi@nao.cas.cn

they are ideal for testing the close connection between the properties of dark matter haloes and the assembly of stellar mass predicted by CDM models. Relatively direct comparison between models and observations is now possible thanks to detailed kinematic analyses of the MW dSphs (e.g. Peñarrubia, Navarro & McConnachie 2008; Strigari et al. 2008; Łokas 2009; Walker et al. 2009; Strigari, Frenk & White 2010; Wolf et al. 2010). Boylan-Kolchin, Bullock & Kaplinghat (2011, 2012) compared observed dSph stellar kinematics to predictions from the Aquarius Project, a set of six *N*-body simulations of dark matter haloes of mass $\sim 10^{12}\,\mathrm{M}_\odot$ (consistent with constraints on the halo mass of the MW; see e.g. fig. 1 of Wang et al. 2015). They concluded that the most massive subhaloes in such simulations, which in typical galaxy formation models would host the most luminous satellites, are always too dense to be dynamically consistent with observations of any of the known MW companions. Boylan-Kolchin et al. (2011) dubbed this discrepancy the 'too big to fail' (TBTF) problem.

Several possible solutions to the problem have been advanced, including alternative forms of dark matter (e.g. Lovell et al. 2012; Vogelsberger & Zavala 2013; Bose et al. 2015), baryon-induced changes in dark halo density profiles (di Cintio et al. 2011; Arraki et al. 2014; Garrison-Kimmel et al. 2013; Brooks & Zolotov 2014) and uncertainties in the mass of the MW halo (Wang et al. 2012; Cautun et al. 2014b). All of these studies use dark matter halo mass as a starting point to select MW analogues in simulations in order to analyse the internal kinematics of their subhaloes. However, galaxy formation involves many complex processes and its outcome depends not only on the present-day halo mass, but also on the formation history of the system. This is an important consideration both for the selection of primary galaxies and for the identification of relevant satellite haloes. Indeed, Sawala et al. (2015) show that huge scatter exists in the relation between the stellar mass of dwarf satellite galaxies and their present-day subhalo mass. Sawala et al. (2014) simulated analogues of the Local Group including full baryonic physics and found that the expulsion of baryons in winds from small dark matter haloes at early times reduced the central density of the haloes in which satellites form enough to solve the TBTF problem.

In this paper we implement the galaxy formation model of Guo et al. (2013) on two *N*-body cosmological simulations and identify MW analogues using the properties of their central galaxies. We compare the halo mass of these MW analogues to the observations, and examine the possibility of dark matter haloes of given mass hosting the MW analogues. We then further analyse the abundance and kinematics of the subhaloes of satellite galaxies selected by their luminosity or stellar mass. At the end we investigate whether selecting MW analogues according to these observables could help solve the TBTF problem.

## 2 SIMULATION AND SEMI-ANALYTIC MODELS

This work makes use of two ΛCDM simulations: a high-resolution zoom simulation, *Copernicus Complexio* (hereafter COCO; Hellwing et al. 2015), and a cosmological volume simulation of lower resolution, Millennium-II (hereafter MS-II; Boylan-Kolchin et al. 2009). The MS-II cube has sidelength $100\,h^{-1}$ Mpc. The particle mass is $m_\mathrm{p} = 6.9 \times 10^6\,h^{-1}\,\mathrm{M}_\odot$ and the force softening scale is $\varepsilon = 1\,h^{-1}$ kpc. It assumes 1-year *Wilkinson Microwave Anisotropy Probe* (*WMAP*-1) cosmological parameters, with a linear power spectrum normalization, $\sigma_8 = 0.9$, and matter density, $\Omega_\mathrm{m} = 0.25$.

COCO simulates a high-resolution comoving volume $V = 2.25 \times 10^4\,h^{-3}\,\mathrm{Mpc}^3$ in the centre of a lower resolution periodic cosmological cube of sidelength $70.4\,h^{-1}$ Mpc using $N_\mathrm{p} = 2374^3$ dark matter particles. This results in a sample of ∼50 haloes of $\sim 10^{12}\,\mathrm{M}_\odot$ at $z = 0$ with high mass ($m_\mathrm{p} = 1.135 \times 10^5\,h^{-1}\,\mathrm{M}_\odot$) and force ($\varepsilon = 230\,h^{-1}$ pc) resolution. Initial density perturbations were generated with the novel *Panphasia* technique (Jenkins 2013) which provides self-consistent and reproducible random phases for zoom-in resimulations across an arbitrary range of resolution.[1]

Unlike MS-II, COCO assumes *WMAP*-7 cosmological parameters ($\Omega_\mathrm{m} = 0.272$, $\Omega_\Lambda = 0.728$, $\sigma_8 = 0.81$ and $n_\mathrm{s} = 0.968$). The slightly different cosmogonies simulated by these two calculations are reflected in the abundances and internal properties of their dark matter haloes. For example, the abundance of MW-mass haloes differs by a few per cent (Boylan-Kolchin et al. 2011). However, the structural and kinematic properties of massive subhaloes in MW haloes are not affected in any significant way (Boylan-Kolchin et al. 2011; Wang et al. 2012; Garrison-Kimmel et al. 2013; Cautun et al. 2014a).

We used stored snapshots (160 for COCO and 68 for MS-II) for Friend-of-Friends (FoF) group finding (Davis et al. 1985) with a linking length equal to 0.2 times the mean interparticle separation. Subhaloes are identified by applying the SUBFIND (Springel, Yoshida & White 2001) algorithm to each FoF group. We define the centre of the FoF group as the potential minimum of the most massive self-bound subhalo. The viral mass, $M_\mathrm{vir}$, is defined as the mass enclosed by a virial radius, $R_\mathrm{vir}$, which we approximate by the radius, $R_{200}$, within which the mean density is 200 times the critical value for closure. The maximum circular velocity of a halo is defined as $V_\mathrm{max} = \max[\sqrt{GM(r)/r}]$ and is attained at radius $r_\mathrm{max}$. For haloes close to the resolution limit, $V_\mathrm{max}$ can be systematically underestimated. To correct for this effect, following Springel et al. (2008), we adjust measurements $V'_\mathrm{max}$ from the simulation to $V_\mathrm{max} = V'_\mathrm{max}(1 + (\varepsilon/r_\mathrm{max})^2)^{0.5}$.

To populate dark matter haloes in the COCO simulation with galaxies, we applied the semi-analytic model recently developed by the Munich Group (Guo et al. 2011, 2013) to their merger trees. This model reproduces many statistical properties of the observed galaxy population, including the abundance of bright satellites around the MW (Guo et al. 2011). There are two processes crucial in understanding the formation of low-mass systems: UV reionization and supernova (SN) feedback. Guo et al. (2011, 2013) adopted a fitting function originally proposed by Gnedin et al. (2004) to describe the baryon fraction as a function of halo mass and redshift. The fitting parameter and the characteristic halo mass beyond which the baryon fraction is close the universal value but below which it rapidly drops with decreasing halo mass are given by Okamoto, Gao & Theuns (2008). For the MS-II, we use the publicly available data from http://www.mpa-garching.mpg.de/millennium.

Guo et al. (2011, 2013) introduced a SN feedback model which depends strongly on the maximum velocity of the subhalo, but the total amount of energy to reheat and eject gas can never exceed the total energy released by Type II SN. For most of the satellites around the MW, the feedback energy saturates at this value. Guo et al. (2011) also showed that SN feedback dominates the formation of relative luminous satellites ($M_V < -11$), while reionization becomes important only for the very faint satellites ($M_V > -11$).

[1] The specific COCO phase information is available on a request from the authors.

In Guo et al. (2011), satellite galaxies within the virial radius of their host are subject to two environmental effects: stripping of their hot gas halo by tides and ram pressure, and tidal disruption of their stellar component. The orbit of the satellite's subhalo in the *N*-body simulation is used to estimate these tidal and ram pressure forces. Once a satellite galaxy loses its parent subhalo, it is considered to merge into the central galaxy unless the density of the host halo at the pericentre of the satellite's orbit exceeds the average baryonic mass density within the half-mass radius of the satellite. In this latter case, cold gas from the disrupted satellite is added to the hot gas halo of the host, and stars from the satellite to a 'stellar halo' component (which is not counted towards the stellar mass of the central galaxy).

In the following sections we describe how we select MW analogues from the resulting mock catalogues and present our analysis of their satellite galaxy populations.

## 3 RESULTS

The particle mass resolution of MS-II is sufficient to study the formation history of haloes more massive than $\sim 10^{10}\,\mathrm{M}_\odot$. Moreover, in our semi-analytic model, the properties of central galaxies in haloes of mass $10^{12}\,\mathrm{M}_\odot$ are converged at the resolution of MS-II. However, the resolution of MS-II is not sufficient to study the internal kinematics of satellites with $V_{\rm max} \lesssim 30\,\mathrm{km\,s^{-1}}$ (Wang et al. 2012). The resolution limit of COCO corresponds to $V_{\rm max} \sim 10\,\mathrm{km\,s^{-1}}$ (Hellwing et al. 2015), corresponding to the least massive satellite galaxies known in the MW system. The smaller volume of COCO yields relatively few MW analogues, however. We therefore use the larger volume of MS-II to study the halo mass distribution of MW analogues selected according to their observable properties, and the higher resolution of COCO to study the internal properties of subhaloes in systems selected in this way.

### 3.1 Halo mass of the Milky Way

In previous works MW analogues have been identified by selecting isolated haloes with mass in a narrow range, typically around $\sim 10^{12}\,\mathrm{M}_\odot$. However, both theoretical work (e.g. Behroozi, Conroy & Wechsler 2010; Guo et al. 2010; Moster et al. 2010; Cautun et al. 2014a) and observational data (e.g. Mandelbaum et al. 2006; Leauthaud et al. 2012) suggest that the scatter in the relation between galaxy mass and host halo mass is large. This raises the question of whether or not a narrow halo mass range is sufficiently representative of the 'MW' galaxy population.

In the following we use galaxy properties predicted by our semi-analytic model to select MW analogues, rather than dark matter halo mass. Our selection is based the stellar mass and morphology of the central galaxy with the following criteria:

$$5 \times 10^{10} < M_* < 7 \times 10^{10}\,\mathrm{M}_\odot \quad (1)$$

and

$$0.05 < M_{\rm bulge}/M_* < 0.4, \quad (2)$$

where $M_*$ is the total stellar mass of the galaxy and $M_{\rm bulge}$ is the stellar mass of the galactic bulge. We have chosen this stellar mass range based on recent observational constraints (e.g. McMillan 2011). The bulge selection is only intended to restrict the sample to disc-dominated galaxies. The actual bulge mass fraction of the MW is uncertain, as is the extent to which the model 'bulge' mass corresponds to the photometrically or kinetically classified 'bulges' of real disc-dominated galaxies. This joint selection yields 566 MW-like galaxies in MS-II and 13 in COCO.

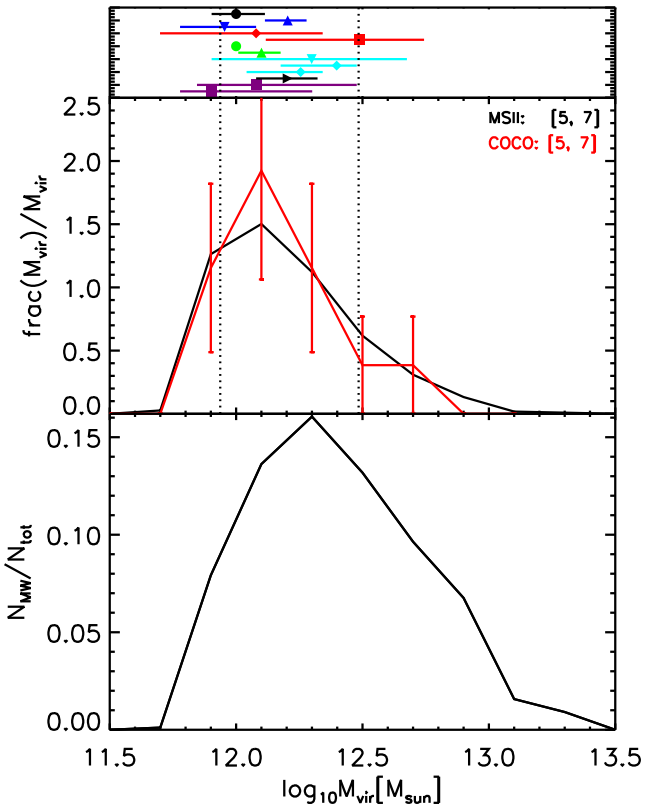


**Figure 1.** Upper panel: collection of measurements of $M_{\rm vir}$ for the MW taken from the literature (see text for details). Middle panel: the distribution of host halo mass for model galaxies with $5 < M_* < 7 \times 10^{10}\,\mathrm{M}_\odot$ and $0.05 < M_{\rm bulge}/M_* < 0.4$ selected in the MS-II (black curves) and COCO (red curves) simulations. Error bars show the Poisson errors for each mass bin. A K–S test supports the hypothesis of a common parent distribution in the MS-II and COCO samples at a confidence level of 0.97. Dotted lines mark the 16th–84th percentile range of the MS-II sample. Bottom panel: the probability for a halo of a given mass to host a galaxy that matches our MW criteria in MS-II.

In Fig. 1, the middle panel shows the distribution of $M_{\rm vir}$ for simulated MW analogues selected according to these criteria. The black curve represents the MS-II sample and the red curve the COCO sample. Although the mass and spatial resolution of the two simulations differ greatly, a Kolmogorov–Smirnov (K–S) test supports the hypothesis that these two samples are drawn from a common parent distribution at a confidence level of 0.97 (roughly within Poisson errors, as shown).

The median halo mass is $1.4 \times 10^{12}\,\mathrm{M}_\odot$, with the 16th to 84th percentile range ($8.6\times\ 10^{11}$–$3.1\times\ 10^{12}\,\mathrm{M}_\odot$) indicated by black dashed lines. A number of observational measurements of $M_{200}$ are shown by symbols with error bars in the top panel of Fig. 1. These measurements have been made using the kinematics of different halo tracers by Xue et al. (2008, black circle), Gnedin et al. (2010, blue upward triangle), Watkins, Evans & An (2010, blue downward triangle), Sakamoto, Chiba & Beers (2003, cyan diamonds, with or without the inclusion of Leo I) and Battaglia et al. (2005, purple squares, assuming a truncated flat model or Navarro–Frenk–White, NFW, model); using the escape velocity of the Large Magellanic Cloud or satellites (Busha et al. 2011, red diamond); using masers by Klypin, Zhao & Somerville (2002, green circle), incorporating

photometric and kinematic data by McMillan (2011, green upward triangle); using abundance matching by Guo et al. (2010, cyan downward triangle); using the escape velocity of halo stars by Piffl et al. (2014, black rightfacing triangle) and using the timing argument of the MW/Andromeda pair by Li & White (2008, red square). Almost all of the measurements in the literature fall between the 16th and 84th percentiles of the distribution predicted by our model. The model predicts that haloes of even higher masses could also host galaxies satisfying our MW selection criteria: 31 per cent of the host haloes in our samples are more massive than $2 \times 10^{12}\,\mathrm{M}_\odot$ and 17 per cent are more massive than $3 \times 10^{12}\,\mathrm{M}_\odot$.

We have tested how a systematic shift in the stellar mass of the MW affects the resulting halo mass distribution by assuming an alternative stellar mass range, $4 \times 10^{10} < M_* < 6 \times 10^{10}\,\mathrm{M}_\odot$. Relative to the peak of the black curve, we find the distribution of $M_{\rm vir}$ shifts to lower mass by ∼0.1 dex. In other words, the host halo mass range does not change much if we reduce the median 'MW' stellar mass by 20 per cent.

The bottom panel of Fig. 1 shows the fraction of all dark matter haloes of a given mass that host a central galaxy satisfying our MW selection criteria. We find that this fraction reaches a maximum of around 16 per cent at $\sim 2 \times 10^{12}\,\mathrm{M}_\odot$. Most of the haloes this mass either host a galaxy substantially more or less massive than the MW, or else host a bulge-dominated galaxy. The fraction of MWs drops rapidly at lower halo masses, and more slowly at higher masses. In general, even in the most favoured range of $M_{200}$, the probability for a halo of any given mass to host a MW analogue is remarkably low. Hydrodynamic simulations of disc galaxies often pre-select haloes from cosmological volumes for 'zoom' resimulations studies based on their mass. Our results indicate that such a selection will always be inefficient. Clearly, other properties of haloes and their individual formation histories also need to be taken into account (Sawala et al. 2015).

### 3.2 Satellite galaxies around the Milky Way

In the last section we have shown that our model predicts a typical halo mass for MW analogues in the same range as recent measurements of the MW galaxy itself. In this section, we will focus on the properties and spatial distribution of satellite galaxies around the MW. As mentioned in Section 2, the mass resolution of the COCO simulation is 60 times higher than that of MS-II, and the spatial resolution is higher by a factor of 4. More than 90 per cent of satellites in MW systems with $V_{\rm max} > 15\,\mathrm{km\,s^{-1}}$ still have their own subhaloes in COCO, which allows us to follow their evolution in detail (see the Appendix). This level of resolution is especially important for studying the internal dynamics and structure of satellite galaxies. For example, their rotation curves can be traced reliably and hence $V_{\rm max}$ can be used as a robust measure of the depth of their potential. Therefore, in the following sections, we only use the COCO simulation to study the properties of satellite systems.

Throughout the paper, we define all galaxies within 280 kpc of each MW analogue to be its satellites. This is the radius within which the census of MW satellite galaxies with $M_V > -9$ is thought to be complete (Koposov et al. 2008; Tollerud et al. 2008).

#### 3.2.1 *Abundance and profile*

Fig. 2 shows cumulative counts of satellite galaxies as a function of *V*-band magnitude around the 13 MW analogues selected from COCO (black curves). The red dot–dashed curve shows the luminosity function of classical satellites around the MW; points with error bars at low luminosity show estimates of the total count of satellites corrected for incompleteness and partial sky coverage by Tollerud et al. (2008), Koposov et al. (2008) and Hargis, Willman & Peter (2014). Tollerud et al. (2008) and Hargis et al. (2014) used simulated subhalo radial distributions for the completeness correction, while Koposov et al. (2008) assumed that the radial distribution of satellites follows an NFW profile. The red dashed curve shows the luminosity function of M31 satellites with $M_V < -10$, the likely completeness limit, from McConnachie (2012). Note that Hargis et al. (2014) adopt a limiting radius of 300 kpc to define satellite galaxies, whereas we adopt a radius of 280 kpc. This slight difference in radius does not affect our main results, since at those large radii subhalo number density declines rapidly (see e.g. Springel et al. 2008; Hellwing et al. 2015). The model predictions are broadly consistent with the data although the slope at the faint end is steeper in the simulations. This demonstrates convergence with the results of Guo et al. (2011), who showed that the bright end of the *V*-band satellite luminosity function for the much larger number of MW analogues in MS-II is also in reasonable agreement with the MW and M31 systems.[2]

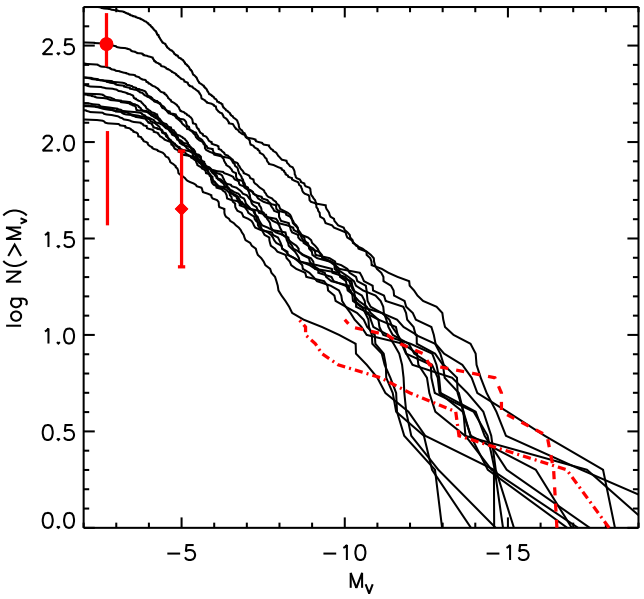


**Figure 2.** Cumulative distribution of *V*-band magnitude for satellite galaxies in each simulated MW system (black curves). Red curves show the equivalent distributions for known bright MW satellites ($M_V < -9$; dot–dashed) and M31 satellites ($M_V < -10$; dashed) (McConnachie 2012). Short vertical lines show estimates of the cumulative number of MW satellites corrected for completeness and sky coverage by Tollerud et al. (2008, dot), Koposov et al. (2008, diamond) and Hargis et al. (2014, no symbol).

Fig. 3 (left-hand panel) compares the galactocentric radial distribution of the most luminous satellites around our MW analogues to those in the real MW system. We restrict this comparison to the 'classical' brightest 12 satellites, using the galactocentric distances given by McConnachie (2012). These observed satellites galaxies are brighter than $M_V \approx -9$, so we select simulated satellite galaxies

[2] The convergence of the MS-II MW satellite luminosity functions, demonstrated here by comparison to COCO, suggests that the semi-analytic treatment of orbits for galaxies whose dark matter haloes are stripped below the resolution of the *N*-body simulation works reasonably well.

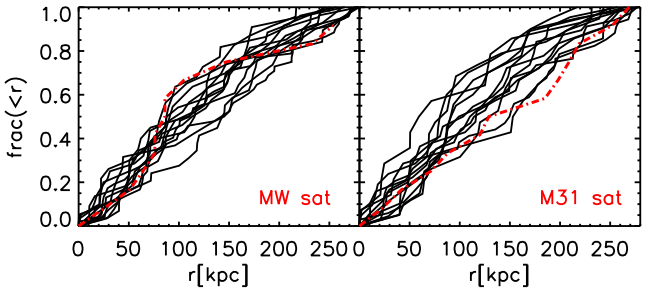


**Figure 3.** Left-hand panel: cumulative radial distribution of the 12 brightest MW satellite galaxies (red dashed curve; McConnachie et al. 2012) compared to those of satellites with $M_V < -9$ in each of our COCO MW analogue systems (black curves). Right-hand panel: cumulative radial distribution of the 12 brightest M31 satellite galaxies (red dashed curve; Yniguez et al. 2014) compared to those of satellites with $M_V < -10$ in the COCO MW analogue systems.

with $M_V < -9$ for this comparison. The MW observations lie within the envelope of the radial distributions from our model.

The right-hand panel of Fig. 3 compares the radial distribution of bright satellites around M31 to those in our model MW analogues. Note that the count of M31 satellites is likely to be complete to $M_V = -10$, slightly brighter than the corresponding limit for the MW – we select simulated galaxies for this comparison accordingly. The observed distances of satellite galaxies to M31 are taken from Yniguez et al. (2014). As in the case of the MW, only galaxies within 280 kpc are counted as satellites for this comparison. In contrast to the MW comparison, the M31 observations lie along the lower envelope of the simulation distribution – most simulated systems are more concentrated than the M31 system. Although the radial distribution of dwarf satellites within 400 kpc of the MW and M31 are very different, as noted by Yniguez et al. (2014), when the comparison is restricted to the bright satellites ($M_V < -9$ and $< -10$ for the MW and M31, respectively) and to a region within 280 kpc, we find that the observed radial distributions of both systems are broadly consistent with our model predictions.

### 3.2.2 *Distribution of* $V_{\rm max}$

In the following we focus on the kinematic properties of satellite galaxies. Recently, detailed kinematic measurements have been carried out for dSphs in the Local Group (e.g. Peñarrubia, Navarro & McConnachie 2008; Strigari et al. 2008; Łokas 2009; Walker et al. 2009; Strigari, Frenk & White 2010, 2014; Wolf et al. 2010), which makes it possible to perform a relatively direct comparison between data and simulations. In particular, stellar kinematics are often used to infer $V_{\rm max}$, which is then used to estimate the gravitational potentials of satellite host dark matter haloes.

$V_{\rm max}$ is not a direct observable, of course, and must be inferred from other properties, such as the mass within a given radius (usually the mass within the half-mass radius, $M_{1/2}$), which in turn is computed from a measured stellar velocity dispersion. To calibrate this procedure, Boylan-Kolchin et al. (2012) computed $V_{\rm max}$ using subhaloes from the Aquarius suite, a series of very high resolution resimulations of dark matter haloes with $M_{200} \sim 10^{12}\,{\rm M}_\odot$. Assuming that the simulated subhaloes together constitute a representative sample of MW-like satellite galaxy hosts, they constructed a theoretical distribution of $V_{\rm max}$ for each real MW satellite. This was done by assigning a weight to the $V_{\rm max}$ of each simulated subhalo,

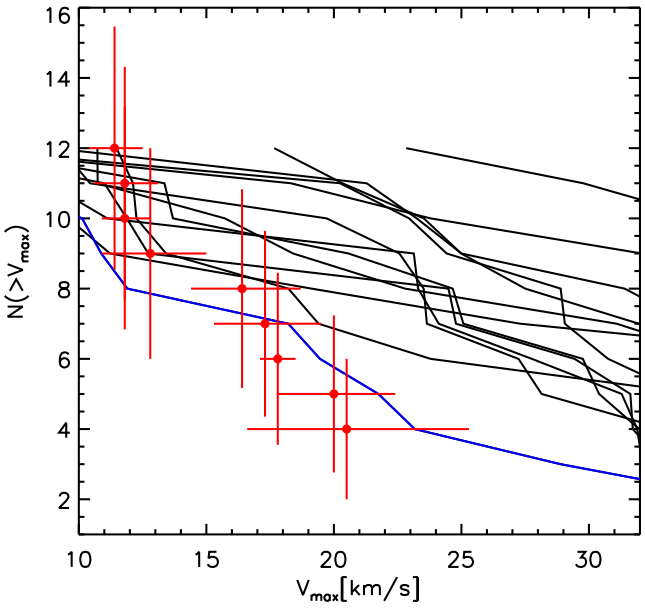


**Figure 4.** Cumulative distribution of maximum circular velocity for the 12 most massive satellite galaxies in each simulated MW system ranked by stellar mass (blue and black curves). Red points show the values of $V_{\rm max}$ for MW satellites given by Boylan-Kochin et al. (2012). The vertical error bars on these points show the Poisson error.

according to how closely its mass within a radius equal to the observed stellar half-mass radius matched the value of $M_{1/2}$ inferred from kinematic observations (for details see Boylan-Kolchin et al. 2012).

Fig. 4 shows the cumulative distribution of $V_{\rm max}$ for the 12 classical brightest satellites around the MW taken from table 2 of Boylan-Kolchin et al. (2012, red symbols with error bars). For comparison to this data, we rank the most massive 12 satellite galaxies of each model MW system according to their stellar mass and construct $V_{\rm max}$ distributions (black and blue lines). The lowest value of $V_{\rm max}$ corresponding to resolved satellites in COCO is about $10\,{\rm km\,s^{-1}}$ (see the Appendix).

Most of the simulated examples overpredict the abundance of satellites with high $V_{\rm max}$ relative to the MW. At $V_{\rm max} \sim 10$–$15\,{\rm km\,s^{-1}}$, predicted subhalo abundances are consistent with the MW system. At $V_{\rm max} \sim 17\,{\rm km\,s^{-1}}$, several model examples still agree with the data within Poisson errors. One out of the 13 simulated MW analogues has a $V_{\rm max}$ distribution consistent with the data (within Poisson errors) over the whole magnitude range considered here. We mark this system with a blue curve in Fig. 4.

The host halo mass of the satellite system represented by the blue curve is $9.7 \times 10^{11}\,{\rm M}_\odot$, around the median of current estimates of the MW host halo masses (Fig. 1). Hence, this is not the least massive halo in our sample. Of all our examples, this system has the lowest abundance of satellites with high $V_{\rm max}$. This may seem somewhat at odds with the conclusions of Wang et al. (2012) and Cautun et al. (2014a), who found that the abundance of subhaloes at high $V_{\rm max}$ is proportional to the host halo mass. Although such a relation holds on average, several factors introduce a large amount of scatter into the correlation. In particular, the luminosity of dwarf galaxies in our semi-analytic model depends strongly on their formation history and not just on their present-day halo mass (e.g. Li et al. 2010). This broadens the relation between luminosity and

halo mass and hence that between luminosity and $V_{\rm max}$. A similar scatter in the properties of low mass galaxies at a fixed halo mass is also found in recent hydrodynamical simulations (Sawala et al. 2015).

### 3.2.3 *Too big to fail?*

Boylan-Kolchin et al. (2011) compared the abundance of dark matter subhaloes as a function of $V_{\rm max}$ in the Aquarius simulations (assumed to be a representative sample of MW host haloes) to the inferred $V_{\rm max}$ distribution of MW satellites. They found that Aquarius predicts significantly more subhaloes with high $V_{\rm max}$ compared to what one could expect from all-sky extrapolation of the available MW data. Specifically, there are only three known satellites galaxies with $V_{\rm max}$ above 30 km s$^{-1}$ (the Large and Small Magellanic Clouds, and the tidally disrupted galaxy in Sagittarius), whereas Aquarius predicts, on average, eight subhaloes with $V_{\rm max} \gtrsim 30$ km s$^{-1}$. This is one of a number of ways to express the TBTF problem mentioned in the Introduction.

Boylan-Kolchin et al. (2012) restated the TBTF problem by comparing the circular velocity profiles of simulated subhaloes to the kinematically best-matching observed MW dwarf spheroidal. Since the instantaneous value of $V_{\rm max}$ for a given subhalo evolves over time (increasing as a subhalo grows, and decreasing as it is tidally stripped), they compare with values $V_{\rm max}(z_{\rm ref})$ at several different reference redshifts ($z_{\rm ref} = 0$, 10, $z_{\rm infall}$, etc.). The idea is that the present-day stellar mass in a subhalo should be tightly correlated with at least one choice of $z_{\rm ref}$. As mentioned in the last section, however, galaxy formation in low-mass haloes can be highly stochastic and can alter the properties of its host halo. Here we will revisit the TBTF problem, taking into account baryonic effects on $V_{\rm max}$.

Fig. 5 shows the fraction of MW analogues which host $N$ or fewer satellites with $V_{\rm max}$ greater than a threshold value (given in the legend). In the top panel, as Boylan-Kolchin et al. (2011, 2012) did, we select the 12 subhaloes with the largest values of $V_{\rm max}$ at $z = 0$. We immediately see the fraction of MW analogues hosting no more than $N = 3$ satellites galaxies with $V_{\rm max} \gtrsim 30$ km s$^{-1}$ is zero, in line with the Aquarius simulations discussed above. However, assuming approximate $\sqrt{N}$ shot noise in the real MW count, we can also note that the fraction of hosts having no more than $N = 5$ subhaloes with $V_{\rm max} \gtrsim 30$ km s$^{-1}$ is 23 per cent. The fraction of 'MW-compatible' systems decreases at a given value of $N$ if we lower the threshold $V_{\rm max}$ (red and cyan curves), and increases if we raise the threshold (blue curve).

Galaxy formation may change the properties of the host halo. A recent study compared Local Group analogues in hydrodynamical and collisionless simulations from the same initial conditions (Sawala et al. 2014) and found that baryonic processes associated with feedback systematically reduce $V_{\rm max}$ for a given subhalo by ∼10–15 per cent. As our simulation is collisionless, it is reasonable to take this effect into account by reducing the $V_{\rm max}$ of each subhalo by 15 per cent. The results are shown in the bottom panel of Fig. 5. We find that after taking into account this effect, the fraction of simulated MW to host few subhaloes with $V_{\rm max}$ greater than a threshold value increases significantly. 35 per cent of the simulated MW analogues have no more than three subhaloes with $V_{\rm max} \gtrsim 30$ km s$^{-1}$.

In summary, in addition to the uncertainty in the appropriate statistical error bar on the observed count of MW satellites, baryonic effects on satellite potentials increase the fraction of simulated ∼$10^{12}$ M$_\odot$ haloes that have an abundances of 'high $V_{\rm max}$' satellites similar to that of the MW system. Therefore, although requiring a lowering host halo mass can alleviate the TBTF problem (Wang et al. 2012; Vera-Ciro et al. 2013; Cautun et al. 2014a), this may not be necessary if baryonic effects on satellite potentials are taken into account. This effect may be crucial for formulating realistic CDM-based theoretical predictions for MW-like satellite systems and their properties.

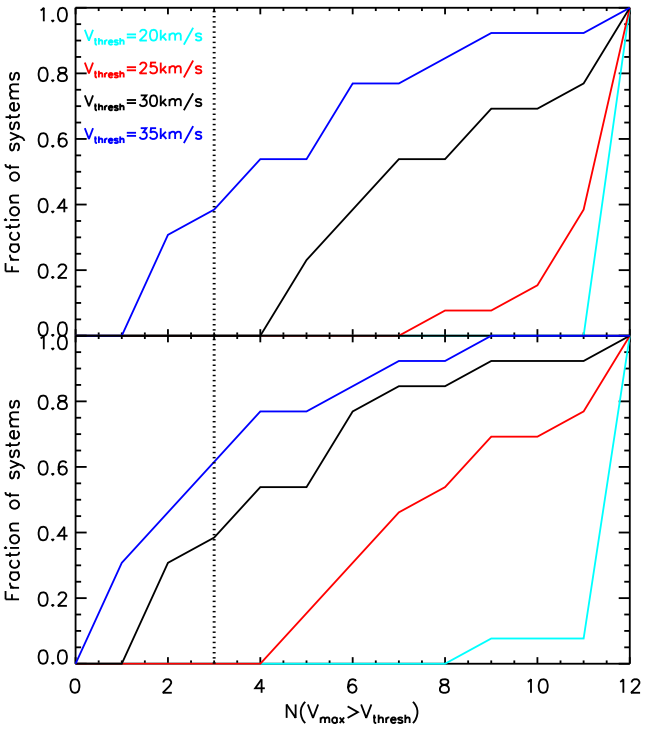


**Figure 5.** Top panel: fraction of MW-like systems in which $N$ or fewer of the top 12 satellites (in order of $V_{\rm max}$) have $V_{\rm max}$ above a particular threshold value, $V_{\rm thresh}$. Different values of $V_{\rm thresh}$ are indicated by colours, as in the legend. Bottom panel: as top panel, but reducing $V_{\rm max}$ for each subhalo by 15 per cent to account for baryonic effects on their potentials as discussed in the text. The dotted vertical line in each panel indicates the threshold of $N = 3$ satellites associated with the TBTF problem in the MW. For example, the point at which the black curve intersects the dotted vertical line in the bottom panel indicates that 35 per cent of simulated systems satisfy the criterion that three or fewer of their top 12 highest $V_{\rm max}$ satellites have $V_{\rm max} > 30$ km s$^{-1}$.

## 3.3 'Dark' substructures

The previous sections demonstrated that our model can reproduce the abundance, radial profile and $V_{\rm max}$ distribution of the satellites in the MW, even though the abundance of subhaloes with high $V_{\rm max}$ is larger than the count of bright satellites observed with the same $V_{\rm max}$. In this section, we will show more quantitatively the diverse properties of satellite galaxies at a given $V_{\rm max}$.

### 3.3.1 $V_{\rm max}$ *versus luminosity*

The top panel of Fig. 6 shows the relation between maximum circular velocity and $V$-band magnitude for satellites in our 13 MW analogues. The predicted median $V_{\rm max}$ is an increasing function of $V$-band luminosity, but the scatter between $V_{\rm max}$ and magnitude, $M_V$, is very large. Even haloes with $V_{\rm max} > 30$ or 20 km s$^{-1}$ can host galaxies fainter than $M_V = -9$ (the approximate limits of completeness

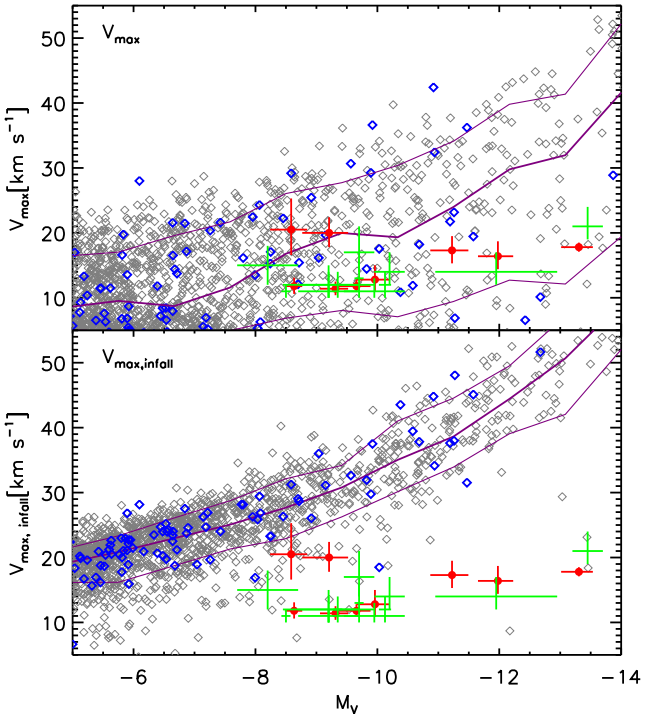


**Figure 6.** Top panel: $V_{\rm max}$ versus $V$-band luminosity for satellites of the MW. Grey diamonds are our model predictions. Blue diamonds highlight satellites of the MW analogue with a $V_{\rm max}$ distribution consistent with the observed data over the whole magnitude range (blue curve in Fig. 4). Thick and thin purple curves give the median and 16–84 per cent range, respectively. Bottom panel: $V_{\rm max,\,infall}$ versus $V$-band luminosity for satellites of the MW. The colour coding and line coding are the same as in the upper panel. Red circles with error bars are the observed MW satellites. Errors in magnitude are taken from Wolf et al.(2010), while those in $V_{\rm max}$ are estimated by Boylan-Kolchin et al. (2012). Green symbols show results for satellite galaxies in M31 as given by Tollerud et al. (2014). We do not include the SMC and LMC in this figure. $V_{\rm max}$ is ∼50–60 km s$^{-1}$ for the SMC (Stanimirović, Staveley-Smith & Jones 2004; Harris & Zaritsky 2006) and >80 km s$^{-1}$ for the LMC (Olsen et al. 2011). For Sagittarius, the appropriate value of $V_{\rm max}$ is hard to determine, because the satellite appears to be strongly perturbed by its interaction with the central potential of the Galaxy.

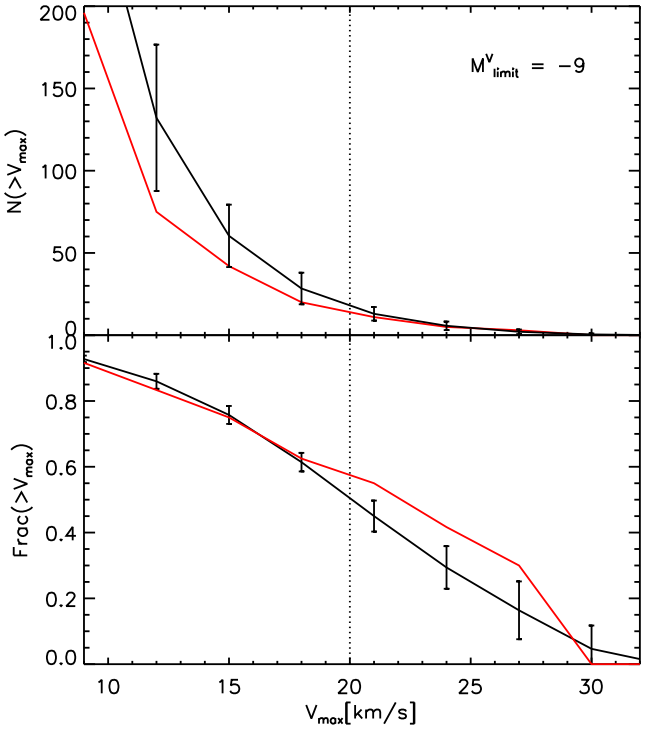


**Figure 7.** Upper panel: number of subhaloes with galaxies fainter than $M_V = -9$ as a function of $V_{\rm max}$. The black curve shows the median value for all 13 MW analogues and the error bars show the 16–84 percentile range. Red curves show the one system that is consistent with the observed MW satellite $V_{\rm max}$ distribution, as shown in Fig. 4. Bottom panel: fraction of the subhaloes hosting galaxies fainter than $M_V = -9$ as a function of $V_{\rm max}$. The colour coding is the same as in the upper panel.

for current all sky surveys of the MW) or −5, suggesting that a significant number of 20–30 km s$^{-1}$ satellites are still to be discovered. Likewise, at a given magnitude, $V_{\rm max}$ covers a wide range. For example, at $M_V \sim -12$, $V_{\rm max}$ varies from 40 to <10 km s$^{-1}$.

This scatter between $V_{\rm max}$ and luminosity stems from the fact mentioned above that the star formation rate history of a dwarf galaxy depends not only on its final halo mass or $V_{\rm max}$, but also on its dark matter mass assembly history (Li et al. 2010; Sawala et al. 2014). The bottom panel shows the relation between final stellar mass and $V_{\rm max}$ measured just before the time of infall. This relation is much tighter than the stellar mass versus present-day $V_{\rm max}$ relation shown in the top panel. This is because the subhaloes hosting satellite galaxies are subject to tidal forces capable of stripping their mass. Galaxies embedded deep inside the potential of the substructures are more condensed and thus more resistant to such stripping, which can lower their central stellar velocity dispersion without necessarily disturbing their surface brightness profile (Peñarrubia et al. 2008; Cooper et al. 2010). Our model implies that in 1/10 of MW analogues ∼1–2 relatively bright ($M_V \lesssim -13$) satellite galaxies may have extremely low values of $V_{\rm max}$ (blue diamonds). In detail, this number will depend sensitively on the depth at which stars are embedded in their host potentials and on the details of tidal stripping.

Fig. 6 also shows the inferred relation between $V_{\rm max}$ and luminosity for MW and M31 satellites. $V_{\rm max}$ is estimated in the same way in both cases (Tollerud et al. 2014). Most of these data lie below the median prediction of the model (thick blue curve), but well within the 16–84 percentile range. Interestingly, however, the most massive satellites in both observational data sets lie furthest below the predicted median relation.

### 3.3.2 *Detection fractions*

In the last section we showed that the scatter between $V_{\rm max}$ and luminosity is large, such that it is possible for relatively massive subhaloes to host a galaxy with luminosity below the current all sky completeness limit. In this section we make an estimate of the fraction of undetected subhaloes as a function of $V_{\rm max}$. For this purpose, we consider $M_V = -9$ to be the current limit of completeness and further assume that this is a hard cut. (In practice this limit is also a function of surface brightness, and survey depth varies across the sky; e.g. Koposov et al. 2008.)

The top panel of Fig. 7 shows the average number of subhaloes hosting galaxies fainter than $M_V = -9$ as a function of $V_{\rm max}$. At 20 km s$^{-1}$ we find a median of 18 subhaloes below this completeness limit. This corresponds to 45 per cent of all the dark matter

substructures of the same $V_{max}$, as shown in the bottom panel. This fraction increases rapidly with decreasing $V_{max}$, such that around 90 per cent of subhaloes (∼250) with $V_{max} > 10\,km\,s^{-1}$ are below the limit. This conclusion holds for the single MW analogue with a $V_{max}$ distribution consistent with MW observations (red curve in Fig. 4).

## 4 CONCLUSIONS

We have applied a semi-analytic galaxy formation model to cosmological *N*-body simulations with sufficiently high resolution to study the properties of MW analogues and their satellite galaxies. Our two simulations give converged predictions for the dark halo mass of the MW, despite a large difference in mass resolution (a factor of 60) and spatial resolution (a factor of 4). Given its stellar mass, the most probable value for the halo mass of the MW according to our model is $1.4 \times 10^{12}\,M_\odot$, with a $1\sigma$ dispersion in the range $8.6 \times 10^{11}$–$3.1 \times 10^{12}\,M_\odot$. This median value is consistent with measurements of the MW halo mass using different dynamical tracers (see Wang et al. 2015, for a summary).

For any given halo mass, the probability of hosting a MW analogue is rather low, with a maximum probability of ∼20 per cent in haloes of mass $\sim 10^{12}\,M_\odot$. This value decreases rapidly with lower and higher host halo mass. This implies that if one wishes to simulate the formation of a MW-like system, halo mass selection alone is not sufficient: other factors such as environment and assembly history are important. We intend to explore the influence of such factors on the formation of MW analogues in future work.

We used the COCO simulation to study the properties of satellites in MW analogues. Our model is able to reproduce both the abundance of satellites as a function of *V*-band luminosity and the radial profile of the bright galaxies ($M_V < -9$). We have compared the $V_{max}$ distribution of the simulated satellites in COCO to inferences of $V_{max}$ from observations. We find one out of 13 $V_{max}$ distributions for our MW analogues overlaps the observed distribution. However, we caution that the 'observed' values of $V_{max}$ are themselves dependent on calibration against collisionless *N*-body simulations.

With this caveat, a conservative upper limit on $V_{max}$ for most known satellite galaxies (excluding the LMC, SMC and Sagittarius) is $\sim 30\,km\,s^{-1}$. The severity of the TBTF problem depends on a number of systematic uncertainties, such as the error assumed on the count of known satellites, the effect of baryonic processes on $V_{max}$ (Sawala et al. 2014, and references therein) and the strength of the correlation between $V_{max}$ and luminosity. Our model shows that reducing $V_{max}$ as suggested by Sawala et al. (2014) is important for matching the observed number of satellites with high $V_{max}$ in haloes hosting MW-like galaxies.

The large scatter between luminosity (stellar mass) and $V_{max}$ is a consequence of the complex formation histories of dwarf galaxies and environmental effects (such as tidal and ram-pressure stripping) acting on dark matter subhaloes. Subhaloes with high $V_{max}$ can host very faint galaxies, and bright galaxies can be hosted by haloes of low $V_{max}$. A significant fraction of subhaloes in our model host galaxies below the approximate all sky completeness limit for present surveys of $M_V > -9$. Around half of our subhaloes with $V_{max} > 20\,km\,s^{-1}$ host galaxies fainter than this limit. Very recently, eight faint satellite galaxy candidates ($-7.4 < M_V < -2.2$) have been discovered by the Dark Energy Survey (The DES Collaboration et al. 2015). The continued discovery of fainter MW companions by deeper surveys will be important for constraining even the massive end of the subhalo mass function and associated tests of the CDM model.

## ACKNOWLEDGEMENTS

We thank Jie Wang and Liang Gao for helpful discussion. QG acknowledges support from the NSFC grant (No. 11133003), the Strategic Priority Research Program 'The Emergence of Cosmological Structure' of the Chinese Academy of Sciences (No. XDB09000000), the 'Recruitment Program of Global Youth Experts' of China, the NAOC grant (Y434011V01), MPG partner Group family and a Royal Society Newton International Fellowship, as well as the hospitality of the Institute for Computational Cosmology at Durham University. APC is supported by a COFUND/Durham Junior Research Fellowship under EU grant [267209] and thanks Liang Gao for support in the early stages of this work under a CAS International Research Fellowship and NSFC grant [11350110323]. CF acknowledges an ERC Advanced Investigator grant COSMIWAY (GA 267291). This work was supported in part by the Science and Technology Facilities Council Consolidated Grant for Durham Astronomy (grant number ST/I00162X/1). This work used the DiRAC Data Centric system at Durham University, operated by the Institute for Computational Cosmology on behalf of the STFC DiRAC HPC Facility (www.dirac.ac.uk). This equipment was funded by BIS National E-infrastructure capital grant ST/K00042X/1, STFC capital grant ST/H008519/1 and STFC DiRAC Operations grant ST/K003267/1 and Durham University. DiRAC is part of the National E-Infrastructure. The COCO simulations were run at the University of Warsaw HPC centre and we would like to thank Maciej Cytowski and Arkadiusz Niegowski for their help with these simulations.

## REFERENCES

Arraki K. S., Klypin A., More S., Trujillo-Gomez S., 2014, MNRAS, 438, 1466
Battaglia G. et al., 2005, MNRAS, 364, 433
Behroozi P. S., Conroy C., Wechsler R. H., 2010, ApJ, 717, 379
Benson A. J., Frenk C. S., Lacey C. G., Baugh C. M., Cole S., 2002, MNRAS, 333, 177
Bose S., Hellwing W. A., Frenk C. S., Jenkins A., Lovell M. R., Helly J. C., Li B., 2015, preprint (arXiv:1507.01998)
Boylan-Kolchin M., Springel V., White S. D. M., Jenkins A., Lemson G., 2009, MNRAS, 398, 1150
Boylan-Kolchin M., Bullock J. S., Kaplinghat M., 2011, MNRAS, 415, L40
Boylan-Kolchin M., Bullock J. S., Kaplinghat M., 2012, MNRAS, 422, 1203
Brooks A. M., Zolotov A., 2014, ApJ, 786, 87
Bullock J. S., Kravtsov A. V., Weinberg D. H., 2000, ApJ, 539, 517
Busha M. T., Marshall P. J., Wechsler R. H., Klypin A., Primack J., 2011, ApJ, 743, 40
Cautun M., Hellwing W. A., van de Weygaert R., Frenk C. S., Jones B. J. T., Sawala T., 2014a, MNRAS, 445, 1820
Cautun M., Frenk C. S., van de Weygaert R., Hellwing W. A., Jones B. J. T., 2014b, MNRAS, 445, 2049
Cooper A. P. et al., 2010, MNRAS, 406, 744
Davis M., Efstathiou G., Frenk C. S., White S. D. M., 1985, ApJ, 292, 371
di Cintio A., Knebe A., Libeskind N. I., Yepes G., Gottlöber S., Hoffman Y., 2011, MNRAS, 417, L74
Efstathiou G., 1992, MNRAS, 256, 43p
Font A. S. et al., 2011, MNRAS, 417, 1260
Garrison-Kimmel S., Rocha M., Boylan-Kolchin M., Bullock J. S., Lally J., 2013, MNRAS, 433, 3539
Gnedin O. Y., Kravtsov A. V., Klypin A. A., Nagai D., 2004, ApJ, 616, 16
Gnedin O. Y., Brown W. R., Geller M. J., Kenyon S. J., 2010, ApJ, 720, L108

Guo Q., White S., Li C., Boylan-Kolchin M., 2010, MNRAS, 404, 1111
Guo Q. et al., 2011, MNRAS, 413, 101
Guo Q., White S., Angulo R. E., Henriques B., Lemson G., Boylan-Kolchin M., Thomas P., Short C., 2013, MNRAS, 428, 1351
Hargis J. R., Willman B., Peter A. H. G., 2014, ApJ, 795, L13
Harris J., Zaritsky D., 2006, AJ, 131, 2514
Hellwing W. A., Frenk C. S., Cautun M., Bose S., Helly J., Jenkins A., Sawala T., Cytowski M., 2015, preprint (arXiv: e-prints)
Jenkins A., 2013, MNRAS, 434, 2094
Kauffmann G., White S. D. M., Guiderdoni B., 1993, MNRAS, 264, 201
Klypin A., Kravtsov A. V., Valenzuela O., Prada F., 1999, ApJ, 522, 82
Klypin A., Zhao H., Somerville R. S., 2002, ApJ, 573, 597
Koposov S. et al., 2008, ApJ, 686, 279
Leauthaud A. et al., 2012, ApJ, 744, 159
Li Y.-S., White S. D. M., 2008, MNRAS, 384, 1459
Li Y.-S., De Lucia G., Helmi A., 2010, MNRAS, 401, 2036
Łokas E. L., 2009, MNRAS, 394, L102
Lovell M. R. et al., 2012, MNRAS, 420, 2318
Macciò A. V., Kang X., Fontanot F., Somerville R. S., Koposov S., Monaco P., 2010, MNRAS, 402, 1995
McConnachie A. W., 2012, AJ, 144, 4
McMillan P. J., 2011, MNRAS, 414, 2446
Mandelbaum R., Seljak U., Kauffmann G., Hirata C. M., Brinkmann J., 2006, MNRAS, 368, 715
Moore B., Ghigna S., Governato F., Lake G., Quinn T., Stadel J., Tozzi P., 1999, ApJ, 524, L19
Moster B. P., Somerville R. S., Maulbetsch C., van den Bosch F. C., Macciò A. V., Naab T., Oser L., 2010, ApJ, 710, 903
Okamoto T., Gao L., Theuns T., 2008, MNRAS, 390, 920
Okamoto T., Frenk C. S., Jenkins A., Theuns T., 2010, MNRAS, 406, 208
Olsen K. A. G., Zaritsky D., Blum R. D., Boyer M. L., Gordon K. D., 2011, ApJ, 737, 29
Parry O. H., Eke V. R., Frenk C. S., Okamoto T., 2012, MNRAS, 419, 3304
Peñarrubia J., Navarro J. F., McConnachie A. W., 2008, ApJ, 673, 226
Piffl T. et al., 2014, A&A, 562, A91
Sakamoto T., Chiba M., Beers T. C., 2003, A&A, 397, 899
Sawala T. et al., 2014, preprint (arXiv:1412.2748)
Sawala T. et al., 2015, MNRAS, 448, 2941
Somerville R. S., 2002, ApJ, 572, L23
Springel V., Yoshida N., White S. D. M., 2001, New Astron., 6, 79
Springel V. et al., 2008, MNRAS, 391, 1685
Stanimirović S., Staveley-Smith L., Jones P. A., 2004, ApJ, 604, 176
Strigari L. E., Bullock J. S., Kaplinghat M., Simon J. D., Geha M., Willman B., Walker M. G., 2008, Nature, 454, 1096
Strigari L. E., Frenk C. S., White S. D. M., 2010, MNRAS, 408, 2364
Strigari L. E., Frenk C. S., White S. D. M., 2014, preprint (arXiv:1406.6079)
The DES Collaboration et al., 2015, ApJ, 807, 50
Tollerud E. J., Bullock J. S., Strigari L. E., Willman B., 2008, ApJ, 688, 277
Tollerud E. J., Boylan-Kolchin M., Bullock J. S., 2014, MNRAS, 440, 3511
Vera-Ciro C. A., Helmi A., Starkenburg E., Breddels M. A., 2013, MNRAS, 428, 1696
Vogelsberger M., Zavala J., 2013, MNRAS, 430, 1722
Wadepuhl M., Springel V., 2011, MNRAS, 410, 1975
Walker M. G., Mateo M., Olszewski E. W., Peñarrubia J., Wyn Evans N., Gilmore G., 2009, ApJ, 704, 1274
Wang J., Frenk C. S., Navarro J. F., Gao L., Sawala T., 2012, MNRAS, 424, 2715
Wang W., Han J., Cooper A., Cole S., Frenk C., Cai Y., Lowing B., 2015, MNRAS, 453, 377
Watkins L. L., Evans N. W., An J. H., 2010, MNRAS, 406, 264
Wolf J., Martinez G. D., Bullock J. S., Kaplinghat M., Geha M., Muñoz R. R., Simon J. D., Avedo F. F., 2010, MNRAS, 406, 1220
Xue X. X. et al., 2008, ApJ, 684, 1143
Yniguez B., Garrison-Kimmel S., Boylan-Kolchin M., Bullock J. S., 2014, MNRAS, 439, 73

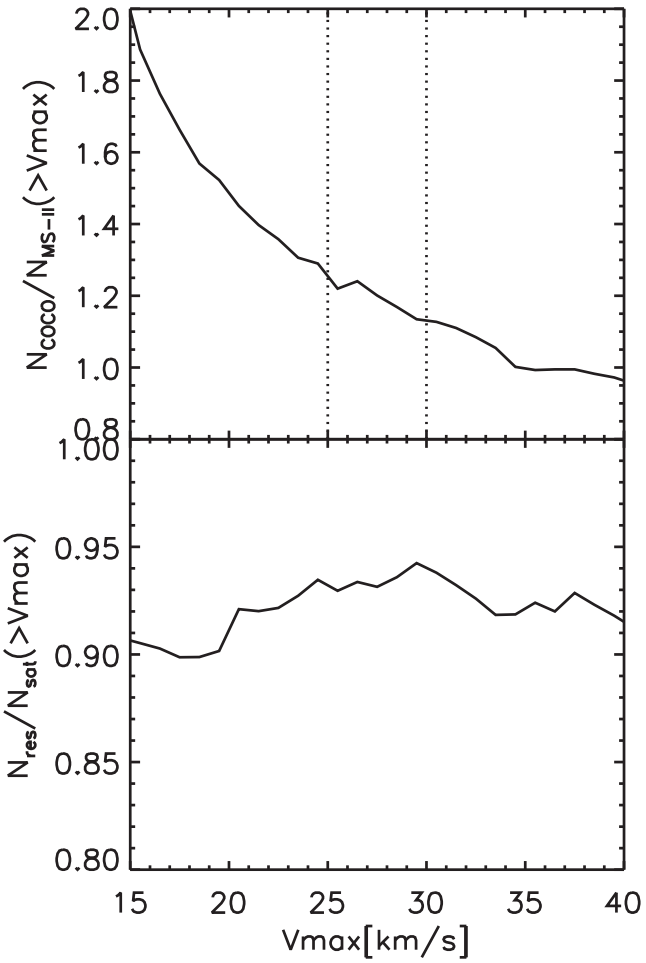


**Figure A1.** Upper panel: the ratio of the cumulative number of subhaloes as a function of $V_{max}$ in the COCO and MS-II simulations. Bottom panel: the ratio of the cumulative number of satellites with and without resolved subhaloes as a function of $V_{max}$.

## APPENDIX A: NUMERICAL CONSIDERATIONS CONCERNING THE MAXIMUM CIRCULAR VELOCITY OF SATELLITES

When haloes fall into larger systems, they orbit around the potential centres as substructures, losing some of their mass to tidal stripping. Some substructures survive for a long time, while others may be disrupted shortly after infall. The finite particle mass of $N$-body simulations sets a minimum mass below which subhaloes cannot be resolved (in SUBFIND, subhaloes must contain at least 20 particles). Since most subhaloes lose mass though tidal stripping, many will eventually fall below this limit and be 'lost' from the simulation. The lower the resolution of the simulation, the more rapidly subhaloes will be lost artificially as a result of this numerical limit. The identification of the surviving substructures is thus affected by numerical resolution.

The MS-II and the COCO simulations differ by a factor of 60 in particle mass and by a factor of 4 in softening length. In Fig. A1 we show the difference in the cumulative number of substructures as a function of maximum circular velocity in the two simulations. The difference is less than 20 per cent at velocities, $V_{max} > 25\,km\,s^{-1}$, but increases very rapidly to 100 per cent at $15\,km\,s^{-1}$. At $20\,km\,s^{-1}$,

MS-II resolves only half of the subhaloes found in COCO. We note that MS-II adopts a higher value of $\sigma_8$ which results in more substructures. Hence, the curve in Fig. A1 is a lower limit on the difference due to resolution. Studies of satellite kinematics with MS-II should be restricted to the regime $V_{\rm max} > 30\,{\rm km\,s^{-1}}$, while most of the MW satellites have $V_{\rm max} < 20\,{\rm km\,s^{-1}}$, except for the LMC, SMC and Sagittarius (e.g. Boylan-Kolchin et al. 2012). It is thus less reliable to use the MS-II to study the properties of satellite of the MW without a very careful treatment of these satellite galaxies whose subhaloes are lost due to resolution.

The semi-analytic galaxy formation model circumvents the resolution limit by allowing satellite galaxies to survive as bound objects for longer than their corresponding *N*-body subhaloes. We refer to these as 'orphan' galaxies, because their parent subhalo has been lost. Their continued survival is determined by analytic calculations of inspiral towards the central galaxy under dynamical friction and the impact of tidal stripping on their stellar profile. The value of $V_{\rm max}$ for orphan galaxies is fixed to that of their parent subhalo at the time it was last resolved. However, since these objects are suffering severe tidal stripping by definition, this estimate of $V_{\rm max}$ is unlikely to be very accurate.

The bottom panel of Fig. A1 shows the fraction of satellite galaxies in our model whose subhaloes are resolved (i.e. are not orphans) as a function $V_{\rm max}$. We find more than 90 per cent of satellite galaxies in COCO are in resolved subhaloes, and thus should have reliable $V_{\rm max}$ measurements. In the main body of the paper we therefore use results from the COCO simulation to study satellite galaxies.

This paper has been typeset from a TEX/LATEX file prepared by the author.